Catalysis Science & Technology

Accepted Manuscript

ROYAL SOCIETY OF CHEMISTRY

www.rsc.org/catalysis

Surfactant controlled magnesium oxide synthesis for base catalysis.

Nicholas F. Dummer[a,b]*, Liam Joyce[a], Harold Ellicot[a], Yijiao Jiang[c]

[a] School of Chemistry, University of Wollongong, Wollongong, NSW 2522, Australia

[b] Now at Cardiff Catalysis Institute, Cardiff University, Cardiff, CF10 3AT, UK

[c] Department of Engineering, Macquarie University, North Ryde, NSW 2109, Australia

* Corresponding author; dummernf@cardiff.ac.uk

Abstract

Magnesium oxide catalysts were used to investigate the influence of novel preparative techniques for surface site control on activity. Firstly, magnesium hydroxide was prepared under hydrothermal conditions with sodium dodecyl sulphate and either sodium hydroxide or a quaternary ammonium ion as morphological and surface controlling agents. Particles with a hexagonal, plate-like morphology were produced with varying dimensions relative to the concentrations of surfactant to ammonium ion. These materials were dehydrated at 420 °C for 2 hours and then characterised by nitrogen adsorption, X-ray diffraction, electron microscopy and the surface hydroxyl density was measured via ^{1}H MAS NMR. Analysis of electron microscopy images of the resulting MgO materials indicted that the morphology of the precursor hydroxide was retained. The MgO materials were then used as catalysts for Knoevenagel condensation of benzaldehyde and ethyl cyanoacetate. The activity of the MgO samples was found to correspond to the surface hydroxyl density; higher activities (ca. 18 mol_{prod} kg^{-1} h^{-1}) were observed for catalysts with a surface hydroxyl density of > 1.3 mmol g^{-1}. Knoevenagel condensation relies greatly on distribution of neighbouring -Mg^{2+} and -O^{2-} sites, the catalysts with a higher density of potentially low coordination –O^{2-} sites resulted in higher product yields. The hydroxyl density was found to be independent of surface area, such that the combination of precipitating agent and surfactant can effectively control crystal growth to tailor the basic active surface of MgO.

Keywords: Magnesium oxide, heterogeneous, catalyst, surfactant, Knoevenagal condensation, quaternary ammonium ion.

Introduction

Magnesium oxide (MgO) continues to attract considerable attention due to a broad range of applications; as an anti-bacterial agent,[1] adsorbent[2] and particularly as a heterogeneous catalyst.[3-7] MgO has proved successful in a number of reactions as both a base catalyst[8-11] for condensation reactions[7, 9, 12] or as a catalyst support.[13-15]

In particular Knoevenagel condensation of active methylene containing compounds and an aldehyde has proved successful over recyclable MgO catalysts[8, 9] when compared to environmentally harmful aqueous bases. The acidic Mg^{2+} site and an aldehyde complexes with an activated methylene compound on a nearby Lewis basic site (O^{2-}).[8] Therefore, the catalytic activity is thought to be largely ascribed to the magnitude of the surface area[9, 16] and hence the morphology plays a large role in controlling this factor.[16]

Recently, the preparation of nano-structured MgO powders has highlighted its versatility and various morphologies have been reported, such as rods,[17-19] thin films,[20, 21] flakes[22, 23] and sheets.[24, 25] The use of surfactants to assist precipitation and promote morphological change in catalyst materials has been well studied. Recent examples concerning MgO preparations show the broad range of surfactant formulations used.[26-29] These include cetyltrimethylammonium bromide[30-32] (CTAB), dioctylsulfosuccinate sodium surfactant (AOT)[26] and ethylenediaminetetraacetic acid disodium salt (EDTA).[28] The surfactants were used to preferentially expose certain crystal planes in order to enhance catalytic activity. Zhu *et al*. reported that MgO nanosheets with a predominately exposed (1 1 1) plane was shown to have greater activity for the condensation reaction of benzaldehyde with acetophenone when compared to cubic MgO crystals comprised exclusively of the (1 0 0) plane.[12] Increases in MgO surface area were reported by Jeon *et al*.[33] with the use of poly(dimethylsiloxane-ethylene oxide) (PDMS-PEO) and resulted in higher activity for biodiesel production. Sodium dodecyl sulphate (SDS), an anionic surfactant has received less attention as a potential additive in the preparation of MgO.[34-36] Ishikawa *et al*.[37, 38] reported the use of SDS as a structural modifier and increased the surface area of Mo-V oxide catalysts. Liu *et al*. [39, 40] posit that the role of the surfactant increases super-saturation and decreases the interfacial energy resulting in facile crystal nuclei formation. However, the use of such a surfactant has, to our knowledge only been used to prepare Mg-based materials which potentially have a higher surface area or greater meso-porosity. Our interest lies in preparing catalysts and understanding their activity, and the versatile basic catalyst MgO is ideal with respect to attempting to control important surface characteristics such as basic sites.

In the present work, we envisaged that a long-chain alkyl ammonium ion would facilitate morphological control and a surfactant could control the relative distribution of micro- and meso-

porous surface areas of hydrothermally prepared materials. Fine control of active site density and potentially the coordination geometry of active surface species is an important albeit challenging aspect of catalyst preparation. Herein, we demonstrate that the novel combination of a quaternary ammonium hydroxide, *tetra*-propyl ammonium hydroxide (TPAOH), as a precipitating agent in the presence of SDS can impart a great influence on the crystal formation of $Mg(OH)_2$. The choice of TPAOH was taken as magnesium hydroxide precipitated by *tetra*-ethyl ammonium hydroxide was largely indistinct from the equivalent NaOH precipitated material. The oxide form, when used as a catalyst illustrates a combinatorial effect of SDS and precipitating agent to control the surface properties and hence the activity of a Knoevenagel condensation reaction.

Experimental

Materials and Equipment

Magnesium Nitrate ($Mg(NO_3)_2.6H_2O$, Ajax Finechem), *tetra*-propylammonium hydroxide solution (TPAOH, 1.0M in H_2O, Sigma-Aldrich), sodium hydroxide mini pearls (NaOH, Ajax Laboratory Chemicals), sodium dodecyl sulfate solution (SDS, 10% in H_2O, Sigma-Aldrich), ethylcyanoacetate (≥98%, Sigma-Aldrich), benzaldehyde (≥99%, Sigma-Aldrich), N,N-dimethylformamide (DMF, anhydrous 99.8%, Sigma-Aldrich), absolute ethanol (99.5% (v/v), Ajax Finechem), chloroform-d ($CDCl_3$ 99.8 atom% D, 0.1% (v/v) TMS), dimethyl sulfoxide-d_6 (DMS, 99.9 atom% D, Sigma-Aldrich) were all used as received.

Hydrothermal synthesis was carried out in a PTFE lined stainless steel reaction vessel (300 mL capacity, Taiatsu Techno). Synthesis reactions were carried out in an isothermal oven (±1 °C, Labec) and calcinations conducted in an open tube furnace (±1 °C, Labec).

Preparation of $Mg(OH)_2$ and MgO

Magnesium hydroxide was prepared via a hydrothermal synthesis route. Typically, 20 mmol of $Mg(NO_3)_2 \cdot 6H_2O$ was dissolved in 100 mL of deionized water and was stirred while the pH of the solution was monitored. To this was added 30 mmol of the precipitating agent; NaOH or TPAOH as a solution in deionized water and stirred for a total of 10 minutes (pH 10.5). As desired, a dilute surfactant solution of SDS (1-4 mmol) was added at 3 minutes and the reaction mixture stirred for a further 7 minutes; upon addition the pH decreased modestly to 10.3. The total reaction volume was kept as 200 mL for all reactions. The reaction mixture was then transferred to a hydrothermal synthesis vessel, sealed and placed in an oven at 175 °C for 24 hours. The resulting precipitate was filtered and washed with deionized water (200 mL) and ethanol (200 mL) to remove traces of the un-reacted species and surfactant. The recovered powder was dried at 80 °C overnight and then ground lightly with a pestle and mortar to break up any aggregates and finally calcined at 420 °C (10 °C/min ramp) for 2 h. Samples are denoted by their synthesis conditions; i.e. sample **A1** = NaOH + 1 mmol SDS formed $Mg(OH)_2$ and sample **B0c** = TPAOH without SDS added and calcined to MgO (Table 1).

Catalytic Reaction

Reactions were carried out at room temperature, nominally 20 °C; magnesium oxide (0.01g) was placed in a reaction vial, to which 1.6 mL of DMF was added. Benzaldehyde (2 mmol) and ethyl cyanoacetate (2 mmol) were then added to the reaction vial and the reaction was stirred for 2 h. Following this, the reaction suspension was centrifuged (5 minutes, 3500 rpm) and the reaction

mixture was analysed by gas chromatography (Shimadzu 2010 plus, Restek Rxi®-5ms 30 m, 0.25 mm I.D., 0.25 μm) and ^{1}H NMR (Varian Inova, Oxford superconducting 500 MHz magnet) to determine the product yield. Catalytic activity was calculated from the moles of product produced per Kg or m^2 of the catalyst per hour.

Characterisation

Powder X-Ray diffraction was performed on the hydroxide and oxide samples and were recorded on a GBC diffractometer (Cu-Kα; K = 0.15406 nm). Thermal analysis (TG-DTA) were recorded on a Shimadzu DTG-60 under nitrogen flow (20 mL/min) with a heating rate of 10 °C/min. Sample morphology was examined by scanning electron microscopy (SEM) on a Jeol JSM-7500FA instrument. The samples were coated with platinum (thickness *ca.* 4 nm) to reduce charging artefacts. Electron dispersive spectroscopy was recorded on a JEOL JSM-7001F microscope, samples were analysed as synthesised. Transmission electron microscopy was conducted with a JEOL JEM-ARM200F STEM instrument operating at 200 kV. Powder samples were suspended in ethanol and agitated with an ultrasonic bath for a short time (10 seconds) before being dropped on to a holey carbon sample holder. Pore character and surface area was estimated by the measurement of nitrogen adsorption and desorption isotherms, measured at -196 °C with an Quantachrome Autosorb-iQ MP instrument. Samples were degassed prior to analysis under vacuum at 200 °C for 2 h. Surface areas were calculated by the Brunauer–Emmett–Teller (BET) method and pore size distributions calculated by *t*-plot, Barrett–Joyner–Halenda (BJH) method using the desorption isotherm and DFT methods, using the silica (cylinder/sphere pore NLDFT) adsorption model.

^{1}H MAS NMR experiments were performed on a Bruker Avance III 300 spectrometer at a resonance frequency of 300 MHz for ^{1}H nuclei. Single-pulse excitation corresponding to a π/2 flip angle with repetition time of 10 s was used. A 4 mm Bruker MAS probe at a sample spinning rate of 12 kHz was used. Typically, 8 transients were acquired using a short pulse width of 3.5 μs. The chemical shifts were measured relative to adamantane as an external standard. The solid-state NMR spectra were processed using the Bruker software TOPSPIN 3.0. Prior to the NMR measurements, the samples were subjected to thermal treatment at 200 °C in vacuum overnight. For comparison a standard sample [Al]MCM-41 was analysed and a surface hydroxyl density of 2.5 mmol g^{-1} was measured.

Results and discussion

Influence of the precipitating agent

Magnesium hydroxide powders were initially synthesised with two precipitating agents; NaOH and TPAOH (Table 1). The powders were dried and analysed by powder XRD (Fig. 1), SEM (Fig. 2) and TG-DTA (Fig. 3). Analysis of the XRD patterns indicates that the precipitating agent has a strong influence on the $Mg(OH)_2$ recovered. Diffraction peaks correspond to the expected hexagonal lattice with the space group $P\bar{3}m1$ (164) (JCPDS no. 00-044-1482) with unit cell parameters (a) = 3.153 Å and (c) = 4.771 Å of the sample **A0**. The sample prepared with NaOH has broad peaks of low intensity which suggests that the hydroxide is comprised of small crystallites. The sharper peaks of the TPAOH prepared material (**B0**) suggests crystallinity has increased with potentially larger grain boundaries. The ratio of the (0 0 1) and (1 0 1) peaks favour the (0 0 1) facet which suggests this material is likely to have large flat crystallites. The influence of extended alkyl chains of the ammonium ion appear to increase the intensity of the (0 0 1) reflection, indicating a promotion in the crystal growth in the (1 0 0) direction i.e. to larger, flatter particles.

Illustrated in Figure 2 are electron micrographs of the two samples; **A0** and **B0**. The dimensions of the materials appear indicative of their XRD patterns; small *ca.* 60 nm diameter particles with a depth of *ca*. 20 nm are observed for NaOH prepared materials. Whereas, for the materials synthesised by TPAOH the particle diameter is larger of *ca.* 1 μm and a depth of *ca.* 80 nm. These particle size dimensions further support the inference that crystal growth has been promoted by adsorption of ammonium ions and the long alkyl chains control this growth.

Thermal analysis (Fig. 3) illustrates the temperature at which dehydration of the hydroxide occurs as the material transitions to the oxide form. The mass loss of all the materials between 300 and 420 °C was recorded to be *ca.* 28 % which closely corresponds to the expected loss of H_2O (31 %). The discrepancy is likely due to the observation that further loss of hydroxyl species requires greater energy (> 500 °C) to remove (Fig. 3). Indeed, the total mass loss from 300 °C to 800 °C is 31.33 % for A0 and 30.93 %. The water loss for the TPAOH sample occurred at a comparable temperature compared to that of the NaOH derived material, however, the transition period was found to be extended. The results suggest that larger particle sizes or the pore characteristics of **B0** require a higher temperature to complete the transition, as greater energy is presumably required to desorb and remove H_2O from the elongated interlayer spaces. Therefore, a temperature of 420 °C was chosen as the calcination temperature for all the samples based on these results to obtain a high surface area; as according to Li et al.[9] higher calcination temperatures result in lower surface areas and typically lower catalytic activity.

Post-calcination, the materials were characterised by powder XRD and nitrogen adsorption. The peaks present in the powder diffraction patterns (Fig. 4) correspond to the cubic MgO (JCPDS no. 45-0946) with the space group $Fm\bar{3}m$ (225) and a lattice parameter of a = 4.222 Å. The low crystallinity of the samples is related to the modest calcination temperature of 420 °C. Sample **A0** has broad diffraction peaks, however, the diffraction pattern for **B0** reveals somewhat sharper peaks which can be ascribed to the crystallinity of the hydroxide precursor as the transformation to the oxide form is topotactic. Table 2 illustrates the calculated crystallite dimensions using the Scherrer equation, with respect to the *hkl* Miller indices (1 1 1), (2 0 0) and (2 2 0) of the samples **A0** and **B0**. The dimensions appear to indicate that for the bulk crystallites the use of TPAOH promotes crystal growth of the $Mg(OH)_2$ in the (1 0 0) direction.

Nitrogen adsorption isotherms are illustrated in Figure 5 and the corresponding BET surface areas are displayed in Table 2. The adsorption isotherms of samples **A0c** and **B0c** are evidently different and conform to type IV and type II isotherms respectively. The high final adsorption volume with **A0c** is likely due to nitrogen condensation of inter-particle voids caused by the increased aggregation found with the smaller particles. Furthermore, the minor hysteresis found with **A0c** in the adsorption isotherm is indicative of a greater relative meso-porosity (Table 2). Overall, sample **A0c** has a higher surface area, which can be related to the smaller particle size when compared to **B0c**. Both samples possess micro-pores of similar volume although the external surface area of **A0c** was found to be higher than for **B0c**. The degree of meso-porosity in MgO materials is considered to be formed through further heat treatment following the release of water from $Mg(OH)_2$.[41] In the case of the MgO of **A0c** the higher relative external surface area may be due how the particles formed and the relative surface roughness acquired during synthesis.

We consider that the alkyl chain length of the *tetra*-propyl ammonium ion has greatly influenced the morphology of the synthesised $Mg(OH)_2$ of sample **B0**. The larger particles resulting from the use of TPAOH suggest that the ammonium ion is able to complex to the -Mg-(OH)-Mg- surface during their formation and effect the crystal growth in the (0 0 1) direction. Quaternary ammonium hydroxides have been used previously in $Mg(OH)_2$ formation by Feldmann et al.[42], however, the metal hydroxide was formed via a polyol-mediated synthesis and is not directly comparable to the present work. Therefore, we consider that the ammonium ion complexes to the -Mg-O^- of the (0 0 1) surface plane, which has the highest relative density of available surface ions. The alkyl chains prevent crystal growth in the (0 0 1) direction, as access is restricted for incoming magnesium hydroxide ions/building units in this direction.

Influence of the surfactant as co-precipitating agent.

Sodium dodecyl sulphate was added as a co-precipitating agent in order to induce an increase of the surface area[33, 34, 37] of $Mg(OH)_2$ and the subsequently formed MgO. Dilute solutions of SDS (containing 1, 2 and 4 mmol) were added to the preparation mixture prior to sealing in a hydrothermal reactor. The magnesium hydroxide materials formed through this reaction were then analysed.

Powder XRD patterns of $Mg(OH)_2$ are illustrated in Figures 6a and b for the respective precipitating agents used; NaOH and TPAOH. In all cases, the crystallite sizes (Table 2) of the samples decreased when SDS has been added. The critical micelle concentration at 25 °C of SDS in water is 8.2 mmol/L; equivalent to 1.6 mmol in 200 mL of water, however this has been shown to increase at higher temperatures.[43] Therefore, we consider that around this region the reaction mixture is affected by incomplete micelle formation under these elevated temperatures competing for surface Mg ions, as crystal growth is perturbed. This is evidenced by the low yield of the **A2** sample prepared with 2 mmol of SDS (Table 1) which appears to be prevented from forming through SDS interacting strongly with $Mg(OH)_2$ building units. Potentially, the lack of competition with an additive such as *tetra*-propyl ammonium ions for surface sites, prevents the formation of sample **A2**. Takenaka *et al*.[44] reported the formation of surfactant $CH_3(CH_2)nCOO$ - Mg complexes as a lamellar mesophase where *n*: 10–20. Further, interactions of surfactant (P123) and Mg were suggested by Rezaei and co-workers.[45] They noted that as the surface density of Mg on the (0 0 1) plane of $Mg(OH)_2$ is the highest of any of the hydroxides surfaces. This suggests that the (0 0 1) plane will be preferentially blocked by the adsorbed, anionic surfactant molecules during the growing process. The XRD patterns indicate that increasing the SDS concentration does not sequentially reduce the crystallinity of the $Mg(OH)_2$ particles. A similar phenomenon was observed by Rezaei and co-workers[45] whereby over the concentration range of the surfactant studied the MgO particle size and surface area were effected most by the median concentration value of those studied. Presumably, the higher the concentration of surfactant results in more stable micelles which are less likely to participate in the surface modification.

Samples were calcined at 420 °C for 2 h and subsequently analysed by N_2 adsorption (Table 2, Fig. S1 supplemental information), XRD (Fig. 7 a and b), SEM (Fig. 8-9). The BET surface areas of the MgO samples (Table 2) indicate that the addition of SDS has a dramatic effect on both the total surface area and the meso-porous surface area. For the samples derived from TPAOH the surface area was increased substantially where 1 and 4 mmols of SDS were added; from 176 $m^2\ g^{-1}$ to *ca.* 332 $m^2\ g^{-1}$ for both **B1c** and **B4c** as evidenced by the adsorption isotherms (Fig. S1). However, with 2 mmol of SDS in the case of **B2c** the surface area is greatly decreased to 55 $m^2\ g^{-1}$ as with sample **A1c** (105 $m^2\ g^{-1}$). Due to the low yield of the sample **A2** no nitrogen adsorption experiments could be performed. In general, the addition of SDS leads to greater micro-pore volume with an increase of BET surface area (Table 2). Where the surface area is reduced as with **A1c** and **B2c** we suggest that the formation of the magnesium hydroxide pre-cursor is greatly disrupted by the formation of SDS

micelles in solution where ca. 1 or 2 mmol is added with NaOH and TPAOH respectively. Potentially, a form of soft-templating could have occurred in the case of **A1** and **B2** as the relative level of meso-porosity has increased.

Interaction between SDS and the alkyl chains of the ammonium ion can occur and lead to competition for surface sites which is not possible in the case of NaOH derived samples. Samples in the **B** series illustrate this competition through the decreased size of the $Mg(OH)_2$ particles formed (Fig. 9) whereas the **A** series remains largely unchanged (Fig. 8). Li *et al*.[26] reported that greater pore volume could be induced in MgO through the use of the surfactant sodium dioctylsulfosuccinate as a soft-template. The $Mg(OH)_2$ primary crystalline building units were thought to form around micelles and upon their removal created void spaces which increased the surface area. The pores size distribution was substantially broadened and meso-pores were detected with diameters of 10-20 nm. This form of soft-templating does not appear to have occurred with SDS under the present conditions apart from **A1c** and **B2c**, which may be due to the size of the micelles[46] or a weaker interaction. Surface contamination from sulphur containing species (SDS) or carbonaceous deposits were discounted with the use of electron dispersive spectroscopy (EDS) (Fig. S2) and thermal analysis of samples **A0** compared to **B4** (Fig. S3).

The XRD patterns (Fig. 7) are indicative of poorly crystalline MgO and the use of SDS resulted in a further loss of crystallinity. Crystallite sizes as determined by the use of the Scherrer equation indicate that the SDS causes smaller crystallite sizes in the **B** series, although the **A** series remains largely unchanged. Electron micrographs (Fig. 8 and 9) of the MgO samples indicate that the particle size of the **B** series has been reduced. In the case of samples in the **A** series the particles are slightly larger on average compared; from 80 - 160 nm for **A0c** to 100 -300 nm for **A1**, 80 – 130 nm for **A2c** and to 95 – 190 nm for **A4c**. Over the **B** series the particles have decreased in diameter; from > 1 μm for **B0c** to 120 – 235 nm for **B1c** to 120 – 730 nm for **B2c** and for **B4c** to 150 – 240 nm. Which suggests that the interaction between SDS, TPAOH and primary $Mg(OH)_2$ building units is disordered with sample **B2**. The larger particles indicate higher TPAOH interaction, where a portion of the added SDS is presumably stabilised as micelles in solution, the smaller particles present suggest a higher degree of SDS interaction as with **B4c**.

Figure 10 illustrates the multifaceted nature of the **B0c** and **B4c** samples through high-resolution transmission electron microscopy. Images were generally acquired from the edge of the particles, particularly in the case of **B0c**; due to the thickness of the particle being > 50 nm. In general, the MgO crystallite sizes that make up the particle are in the range of 2-4 nm and orientated largely in the (1 1 1) plane for **B0c**. However, crystallites were found to be orientated at the surface in both (1 1 1) and (1 0 0) directions for **B4c**. According to XRD the crystallite dimensions calculated (Table 2) are comparable to those observed with TEM for sample **B4c**. However, the bulk domains of **B0c** could

not be surveyed in the same manner due to the thickness of the particles and potentially larger crystallites may reside there. Analysis of the TEM images suggest that the formation of the large **B0** particles is less random than in the case of **B4**; where increased competition for surface sites between the TPAOH and SDS may impose disorder in the formation of the final particle. We consider that this supports the differences observed in the transition temperatures between **A0** and **B4** (Fig S3) and occurs due to the energy required to form the oxide where the structure is heterogeneous.

Surface hydroxyl density was measured from analysis of ^{1}H MAS NMR of the MgO samples with the exception of **A2c** (Table 3 and Fig. S4). Samples were heated under vacuum and then dosed with hydrogen to form hydroxyl species on the surface. Therefore, peaks in the spectra illustrated in Fig S4 are integrated to obtain a peak area which can be used to calculate the hydroxyl density of the MgO surface and this provides an indication of the degree of basicity that the samples possess. The density of surface hydroxyls, however, cannot distinguish the coordination environment of the corresponding surface $–O^{2-}$ ions. For samples precipitated by NaOH the hydroxyl density per gram was found to increase as the SDS concentration increases (Table 3). We, therefore, consider that the basicity of the **A4c** sample is higher than the **A0c** sample. The influence of the SDS in this case appears to have promoted a relative increase of microporous surface area with greater step and kink surface density which has potentially exposed a greater number of $–O^{2-}$ sites. Competition between TPAOH and SDS has in general effected the formation of $Mg(OH)_2$ by reducing the surface hydroxyl density of the MgO material. The increased occurrence of MgO crystallites of the calcined samples that are orientated in the (1 0 0) direction from TEM analysis indicates that the $–O^{2-}$ site density is reduced. The implications of such surface control are significant and are particularly advantageous in order to refine preparative conditions that result in efficient catalyst materials.

Catalytic reaction

The MgO samples were tested for their activity with the condensation of benzaldehyde and ethyl cyanoacetate at room temperature (Table 3). Knoevenagel condensation reactions over MgO[5] require a high density of basic sites for high activity where the combination of neighbouring $–Mg^{2+}$ and $–O^{2-}$ complex to the incoming reactants.[9] The reactant conversion data illustrated in Table 3 suggests that this is indeed the case over the present samples where the activity per kg of catalyst is relatively higher when the surface hydroxyl density is > 1 mmol g^{-1} (Table 3) as with sample **A4c**. The surface areas of the samples do not share such a relationship with the hydroxyl density, which is largely independent of activity; particularly considering samples **A1c** and **B2c**. These samples have low surface areas (105 and 55 m^2 g^{-1} respectively) but relatively high activity compared to the other catalysts (16.35 and 15.50 mol Kg^{-1} h^{-1} respectively). Therefore, catalytic activity per mass of catalyst (Table 3) was used to compare the samples. From this information we can attempt to correlate the

morphology, surface area and surface hydroxyl density of the MgO catalysts and identify desirable features of the MgO surface for Knoevenagel condensation reactions.

The density of surface hydroxyls were selected in order to highlight the requirement of complimentary basic sites in this condensation reaction. Accordingly, the activity of the two groups in general emphasises that a high surface hydroxyl density increases activity. In the case of group **A** the activity increases with increasing SDS concentration. Whereas, over samples in group **B** the activity generally (excluding **B2c**) decreases with increasing SDS concentration, with a corresponding general decrease in surface hydroxyl density (Table 3). We consider the concentration of SDS greatly affects the formation of the $Mg(OH)_2$ samples i.e. **A1** and **B2** the surface hydroxyl density per m^2 is high despite a low overall surface area. Crucially, above a surface hydroxyl density of ca. 1.3 mmol g^{-1} the activity is improved appreciably. Table 2 illustrates that adding SDS has increased the relative meso-porous nature of samples **A1c** and **B2c** apparently resulting in the higher surface hydroxyl density per surface area. However, the high surface hydroxyl density as measured by NMR in this case cannot distinguish the coordination geometry of the –OH species. Despite this we consider that above 1 mmol g^{-1} the coordination geometry of the $–O^{2-}$ species is potential different i.e. in a low coordination environment due to the higher activity where complimentary $–Mg^{2+}$ and $–O^{2-}$ sites are in greater number.

Concurrent adsorption of benzaldehyde through its C=O group on Mg^{2+} sites and adsorption of ethyl cyanoacetate via H-bonding to O^{2-} sites will improve the catalytic activity. Where the surface hydroxyl density is highest the surface facilitates adsorption of ethyl cyanoacetate and the condensation reaction can proceed efficiently. Analysis of the TEM of samples **B0c** and **B4c** (Fig. 10), the increase of exposed surface MgO crystallites orientated in the (1 0 0) direction support the inference that in combination with TPAOH, SDS decreases the surface hydroxyl density through directing crystal growth. The combination of diverse exposed surface facets and the lowered with surface hydroxyl density of **B4c** compared to **B0c** may rationalise the lower activity observed. Therefore, the combination of SDS and TPAOH has influenced the formation of MgO resulting in an improved surface area, although with a reduced catalytically active surface through decreases in the density of complimentary $-Mg^{2+}$ $-O^{2-}$ basic pair sites i.e. those found more on (1 1 1) surfaces. Where SDS can influence the crystal growth of the forming $Mg(OH)_2$ in the presence of NaOH; or reduced completion by alkyl chains of TPAOH for example, the surface is more suitable to such condensation reactions. Therefore, this approach may find wider application in other catalytic reactions where control of basic surface sites is desirable.

Conclusions

Fine synthetic control of active sites, their density and strength is a crucial part of catalysis and we envisaged that the versatile, basic MgO is an ideal candidate to investigate and achieve this. Catalyst samples were prepared by heat treating $Mg(OH)_2$ which was synthesised using different precipitating agents and surfactant concentrations. The influence of the primary precipitating agent indicated that the quaternary alkyl chains present on an ammonium ion were able to direct particle growth resulting in significantly increased particle size. A surfactant was used in combination with the quaternary alkyl ammonium ion to further influence the crystallite growth and surface characteristics. According to NMR analysis of the surface hydroxyl density, increasing the surfactant concentration resulted in an increase of basic $-O^{2-}$ sites with NaOH precipitated $Mg(OH)_2$. Conversely, the combination of TPAOH and SDS resulted in materials with a lower density of hydroxyl sites. We consider that this arises through competitive adsorption of SDS and TPAOH on the surface of the forming $Mg(OH)_2$ units, resulting in a greater concentration of surface exposed (1 0 0) facets. The increase of hydroxyl sites increased the catalytic Knoevenagel condensation activity of benzaldehyde and ethyl cyanoacetate. Increased adsorption of ethyl cyanoacetate on the higher relative density of $-O^{2-}$ sites facilitated higher reaction rates and was found to be independent of catalyst surface area. We consider that control of surface basicity via the use of targeted concentrations of precipitating agents such as NaOH or TPAOH and surfactants can have great benefits for the field of base catalysis and beyond.

Acknowledgments

The authors are very grateful to the University of Wollongong and the Centre for Medical and Molecular Bioscience for funding and acknowledge the use of the facilities and the assistance of Gilberto Casillas-Garcia at the UOW Electron Microscopy Centre. This research used equipment funded by the Australian Research Council (ARC) – Linkage, Infrastructure, Equipment and Facilities (LIEF) grant LE120100104 located at the UOW Electron Microscopy Centre. The authors would also like to acknowledge the Wollongong Isotope Geochronology Laboratory (UOW) for facilities to collect nitrogen adsorption data.

References

1. J. Sawai, H. Kojima, H. Igarashi, A. Hashimoto, S. Shoji, T. Sawaki, A. Hakoda, E. Kawada, T. Kokugan and M. Shimizu, *World J. Microbiol. Biotechnol*., 2000, **16**, 187-194.

2. C. Gao, W. Zhang, H. Li, L. Lang and Z. Xu, *Cryst. Growth Des*., 2008, **8**, 3785-3790.

3. S. Malinowski, S. Szczepanska and J. Sloczynski, *J. Catal*., 1967, **7**, 68-75.

4. J. L. Lemberton, G. Perot and M. Guisnet, *J. Catal*., 1984, **89**, 69-78.

5. H. Moison, F. Texier-Boullet and A. Foucaud, *Tetrahedron*, 1987, **43**, 537-542.

6. J. S. J. Hargreaves, G. J. Hutchings and R. W. Joyner, *Catal. Today*, 1990, **6**, 481-488.

7. A. B. Patil and B. M. Bhanage, *Catal. Commun*., 2013, **36**, 79-83.

8. H. Moison, F. Texier-Boullet and A. Foucaud, *Tetrahedron*, 1987, **43**, 537-542.

9. C. Xu, J. K. Bartley, D. I. Enache, D. W. Knight and G. J. Hutchings, *Synth.*, 2005, 3468-3476.

10. T. Selvamani, T. Yagyu, S. Kawasaki and I. Mukhopadhyay, *Catal. Commun*., 2010, **11**, 537-541.

11. J. K. Bartley, C. Xu, R. Lloyd, D. I. Enache, D. W. Knight and G. J. Hutchings, *Appl. Catal., B*, 2012, **128**, 31-38.

12. K. Zhu, J. Hu, C. Kübel and R. Richards, *Angew. Chem. Int. Ed*., 2006, **45**, 7277-7281.

13. A. Tompos, J. L. Margitfalvi, E. G. Szabó, Z. Pászti, I. Sajó and G. Radnóczi, *J. Catal*., 2009, **266**, 207-217.

14. M. Khajenoori, M. Rezaei and F. Meshkani, *Chem. Eng. & Tech*., 2014, **37**, 957-963.

15. P. J. Miedziak, H. Alshammari, S. A. Kondrat, T. J. Clarke, T. E. Davies, M. Morad, D. J. Morgan, D. J. Willock, D. W. Knight, S. H. Taylor and G. J. Hutchings, *Green Chem.*, 2014, **16**, 3132-3141.

16. N. Sutradhar, A. Sinhamahapatra, S. K. Pahari, P. Pal, H. C. Bajaj, I. Mukhopadhyay and A. B. Panda, *J. Phys. Chem. C*, 2011, **115**, 12308-12316.

17. Z. Cui, G. W. Meng, W. D. Huang, G. Z. Wang and L. D. Zhang, *Mater. Res. Bull*., 2000, **35**, 1653-1659.

18. Y. Li, M. Sui, Y. Ding, G. Zhang, J. Zhuang and C. Wang, *Adv. Mater*., 2000, **12**, 818-821.

19. L. Yan, J. Zhuang, X. Sun, Z. Deng and Y. Li, *Mater. Chem. Phys*., 2002, **76**, 119-122.

20. V. Matias, J. Hanisch, E. J. Rowley and K. Guth, *J. Mater. Res*., 2009, **24**, 125-129.

21. W. B. Wang, Y. Yang, A. Yanguas-Gil, N. N. Chang, G. S. Girolami and J. R. Abelson, *Appl. Phys. Lett.*, 2013, **102**, 101605_1-101605_4.

22. M. A. Shah and A. Qurashi, *J. Alloys and Compounds*, 2009, **482**, 548-551.

23. Y. Zhang, M. Ma, X. Zhang, B. Wang and R. Liu, *J. Alloys and Compounds*, 2014, **590**, 373-379.

24. T. Selvamani, T. Yagyu, S. Kawasaki and I. Mukhopadhyay, *Catal. Commun*., 2010, **11**, 537-541.

25. T. Selvamani, A. Sinhamahapatra, D. Bhattacharjya and I. Mukhopadhyay, *Mater. Chem. Phys.*, 2011, **129**, 853-861.

26. X. Li, W. Xiao, G. He, W. Zheng, N. Yu and M. Tan, *Colloids Surf., A*, 2012, **408**, 79-86.

27. F. S. H. Simanjuntak, S. R. Lim, B. S. Ahn, H. S. Kim and H. Lee, *Appl. Catal., A*, 2014, **484**, 33-38.

28. F. Wang, N. Ta and W. Shen, *Appl. Catal., A,* 2014, **475**, 76-81.

29. L. Zhang, W. Zhu, H. Zhang, S. Bi and Q. Zhang, *RSC Adv.*, 2014, **4**, 30542-30550.

30. A. Ganguly, P. Trinh, K. V. Ramanujachary, T. Ahmad, A. Mugweru and A. K. Ganguli, *J. Coll. Inter. Sci.*, 2011, **353**, 137-142.

31. H. Dhaouadi, H. Chaabane and F. Touati, *Nano-Micro Lett*., 2011, **3**, 153-159.

32. N. K. Nga, P. T. T. Hong, T. D. Lam and T. Q. Huy, *J. Colloid Interface Sci*., 2013, **398**, 210-216.

33. H. Jeon, D. J. Kim, S. J. Kim and J. H. Kim, *Fuel Processing Technology*, 2013, **116**, 325-331.

34. H. Dong, Z. Du, Y. Zhao and D. Zhou, *Powder Technology*, 2010, **198**, 325-329.

35. Z. Yan, R. Bao, C. M. Busta and D. B. Chrisey, *Nanotechnology*, 2011, **22**, 265611-265618.

36. T. Wang, Y. Xu, Q. Su, R. Yang, L. Wang, B. Liu, S. Shen, G. Jiang, W. Chen and S. Wang, *Mater. Lett*., 2014, **116**, 332-336.

37. S. Ishikawa, X. Yi, T. Murayama and W. Ueda, *Appl. Catal. A: Gen*., 2014, **474**, 10-17.

38. S. Ishikawa, X. Yi, T. Murayama and W. Ueda, *Catal. Today*, 2014, **238**, 35-40.

39. C. Liu, X. Ji and G. Cheng, *Appl. Surf. Sci.*, 2007, **253**, 6840-6843.

40. C. Liu, D. Ma, X. Ji, S. Zhao and S. Li, *Appl. Surf. Sci*., 2011, **257**, 4529-4531.

41. Z. Ling, M. Zheng, Q. Du, Y. Wang, J. Song, W. Dai, L. Zhang, G. Ji and J. Cao, *Solid State Sci.*, 2011, **13**, 2073-2079.

42. C. Feldmann, S. Ahlert, J.-H. Sachse and I. Stahl, EP1867605A1, 2007.

43. P. L. O. Volpe and E. A. S. Filho, *Thermochimica Acta*, 1995, **257**, 59-66.

44. S. Takenaka, S. Sato, R. Takahashi and T. Sodesawa, *Phys. Chem. Chem. Phys*., 2003, **5**, 4968-4973.

45. M. Rezaei, M. Khajenoori and B. Nematollahi, *Mater. Res. Bull*., 2011, **46**, 1632-1637.

46. N. J. Turro and A. Yekta, *J. Am. Chem. Soc*., 1978, **100**, 5951-5952.

Tables and Figures

Table 1. Sample preparation conditions, yield of $Mg(OH)_2$ samples.

Sample Name	Precipitating agent	SDS (mmol)	Yield[a] (%)
A0	NaOH	0	35.2
A1		1	39.7
A2		2	1.9
A4		4	32.3
B0	TPAOH	0	41.2
B1		1	42.2
B2		2	42.1
B4		4	36.3

[a] based on the moles of $Mg(NO_3)_2$

Table 2. Textural properties of the MgO samples

Sample Name	S_{BET} ($m^2\ g^{-1}$)	S_{ext} [a] ($m^2\ g^{-1}$)	S_{micro} [a] ($m^2\ g^{-1}$)	V^a_{micro} (cc g^{-1})	V^b_{DFT} (nm)	Crystallite size[c] (nm)		
						(111)	(200)	(220)
A0c	268	133	134	0.087	0.23	5.4	5.5	5.7
A1c	105	80	25	0.031	0.113	4.0	5.5	5.1
A2c	-	-	-	-	-	6.1	5.2	5.3
A4c	296	80	216	0.134	0.213	5.5	5.7	5.3
B0c	176	28	148	0.082	0.108	12.5	9.7	7.9
B1c	332	84	248	0.126	0.209	6.9	5.4	5.2
B2c	55	48	7	0.003	0.059	7.2	6.3	5.5
B4c	331	47	284	0.158	0.213	7.0	5.7	5.2

[a] Surface areas and micro-pore volume calculated with *t*-plot; [b] pore volume calculated by DFT; [c] estimated with Scherrer equation.

Table 3. Catalytic activity[a] of the MgO samples for Knoevenagel condensation[b]

Sample Name	Surface hydroxyl density[c] (mmol g^{-1})	Surface hydroxyl density[d] (µmol m^{-2})	X_c[e] (%)	Activity[f]	
				$mol_{prod.}\ h^{-1}\ kg_{cat}^{-1}$	$mmol_{prod.}\ h^{-1}\ m^{-2}{}_{cat}$
A0c	0.77	2.9	84.0	16.80	62.70
A1c	1.08	10.3	81.8	16.35	155.72
A2c	-	-	-	-	-
A4c	1.39	4.7	93.3	18.67	63.06
B0c	0.83	4.7	86.2	17.24	97.95
B1c	1.05	3.2	75.0	15.01	45.20
B2c	0.60	10.9	77.5	15.50	281.87
B4c	0.46	1.4	76.1	15.21	46.00

[a] at 2 h; [b] 10 mg catalyst, benzaldehyde (2 mmol) and ethyl cyanoacetate (2 mmol) in DMF (1.6 mL) at room temperature; [c] measured by ^{1}H MAS NMR; [d] calculated from BET surface area; [e] conversion; blank reaction conversion 10.1 %; [f] experimental error was determined to be ± 5% according to standard deviation.

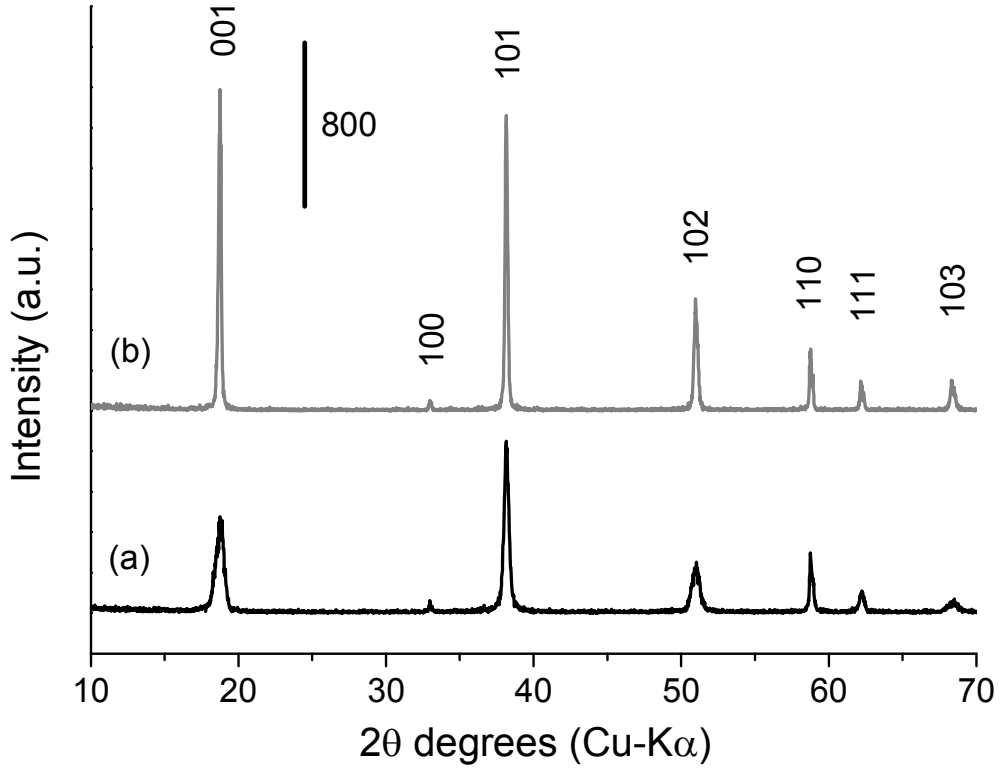

Fig.1. Powder XRD patterns of $Mg(OH)_2$ samples synthesised with different precipitating agents; (a) **A0** and (b) **B0**.

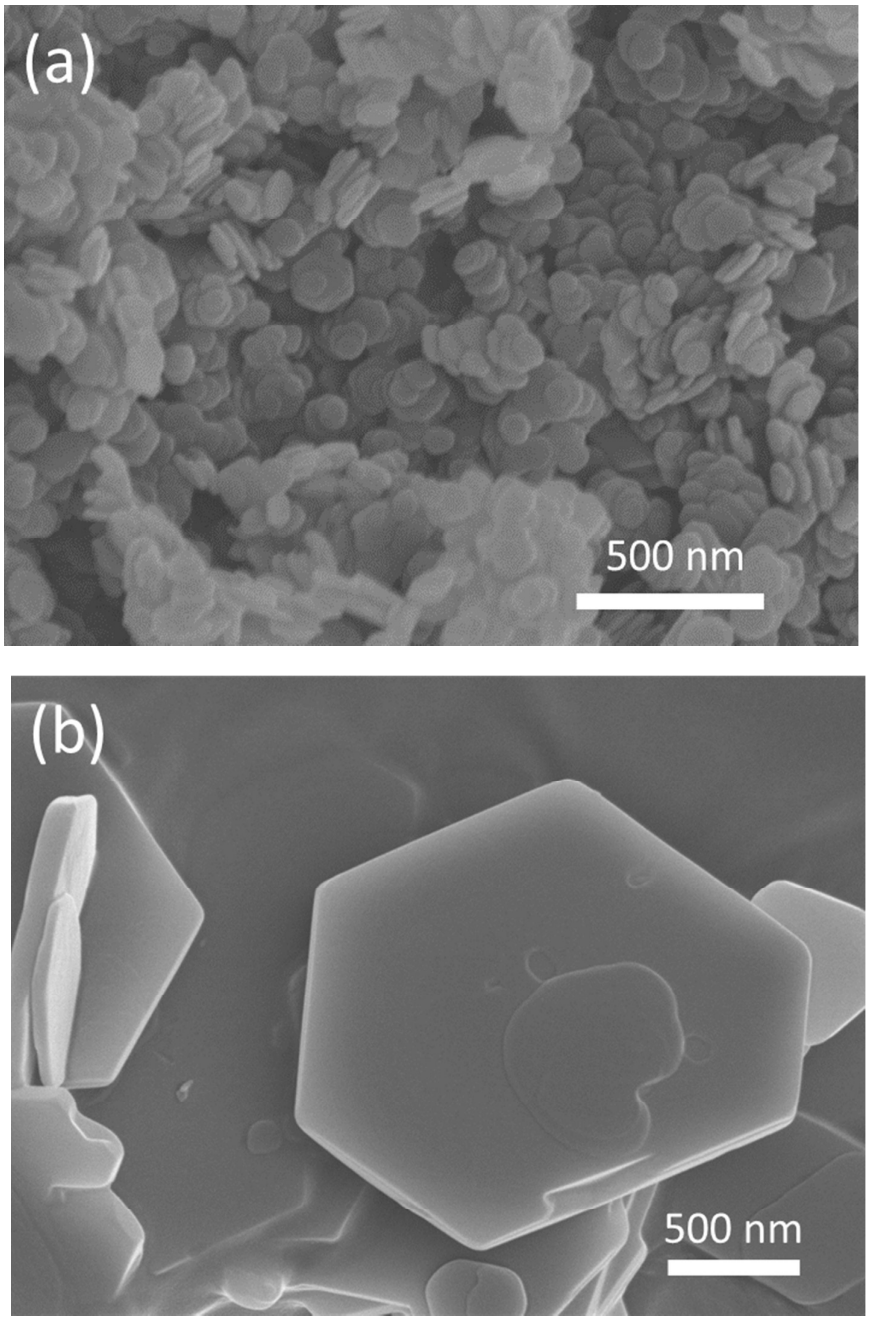

Fig. 2. SEM images of $Mg(OH)_2$ samples (a) **A0** and (b) **B0**.

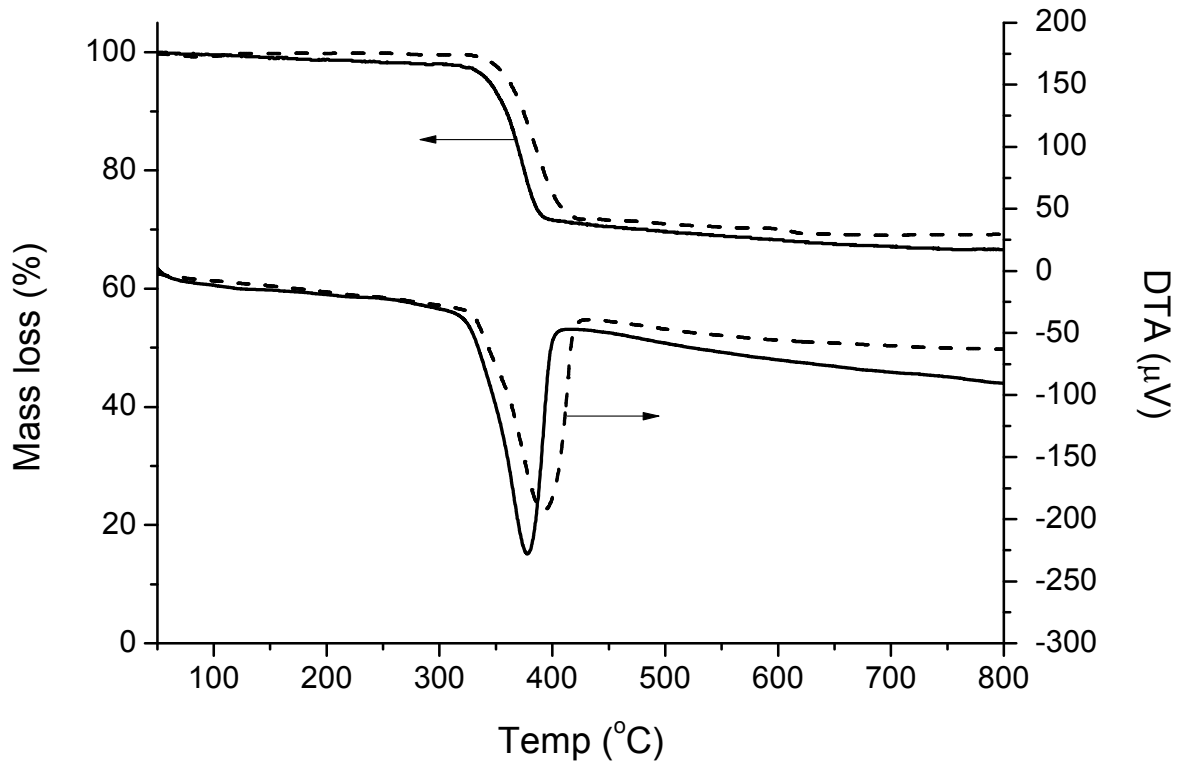

Fig. 3. Thermal analysis of $Mg(OH)_2$ samples **A0** (black lines) and **B0** (dashed lines) as the precipitating agents.

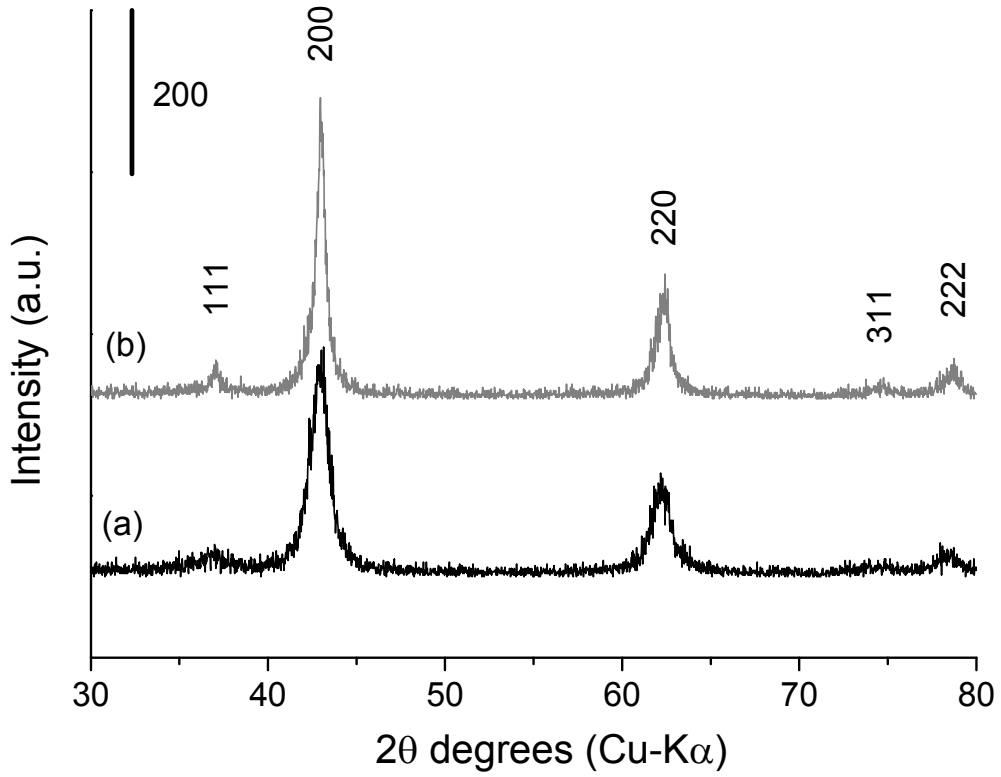

Fig. 4. Powder XRD patterns of MgO samples synthesised with different precipitating agents; (a) **A0c** and (b) **B0c** calcined at 420 °C for 2 h.

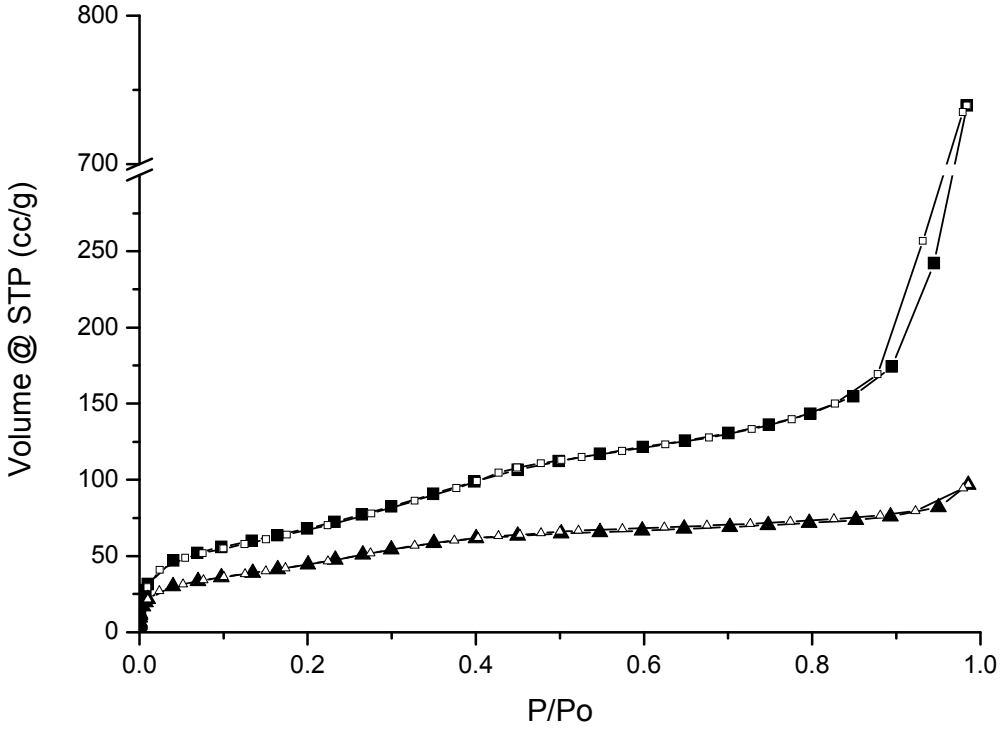

Fig. 5. N_2 Adsorption isotherms for MgO samples synthesised with different precipitating agents, closed symbols; adsorption and open symbols; desorption; (■) NaOH and (▲) TPAOH calcined at 420 °C for 2 h.

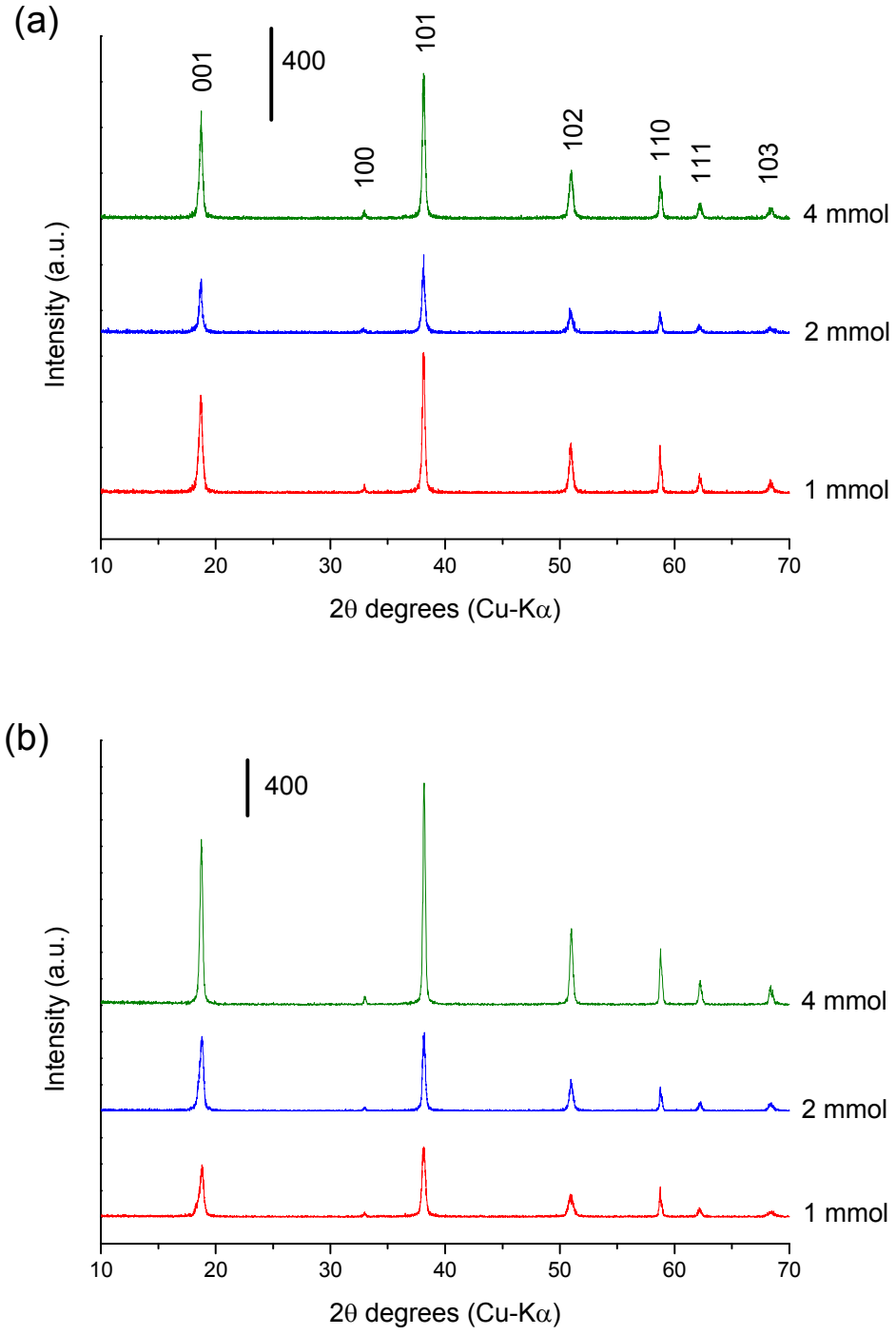

Fig. 6. Powder XRD patterns of $Mg(OH)_2$ samples synthesised with different precipitating agents and different amounts of SDS; (a) NaOH and (b) TPAOH

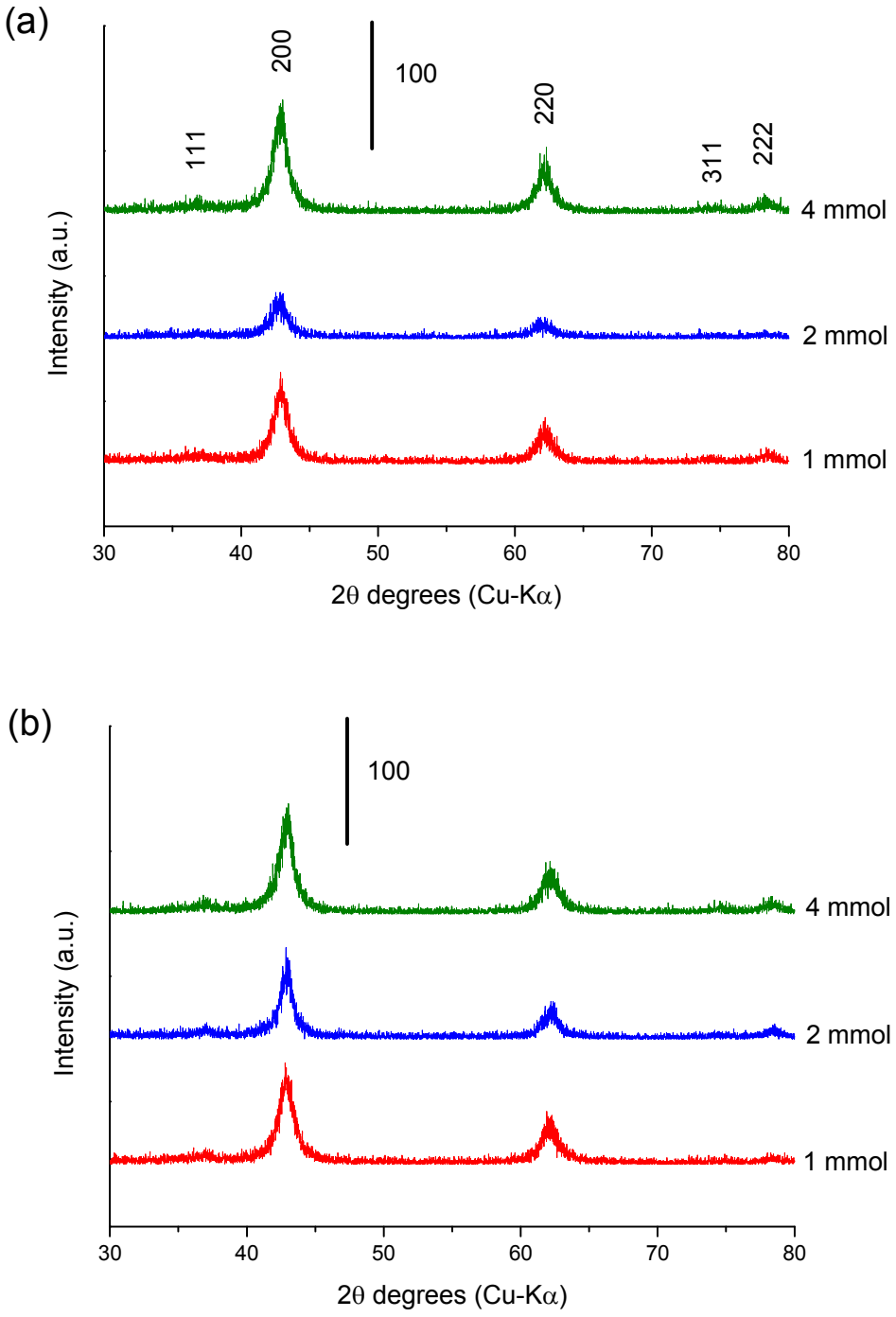

Fig. 7. Powder XRD patterns of MgO samples synthesised with different precipitating agents and different amounts of SDS; (a) NaOH and (b) TPAOH.

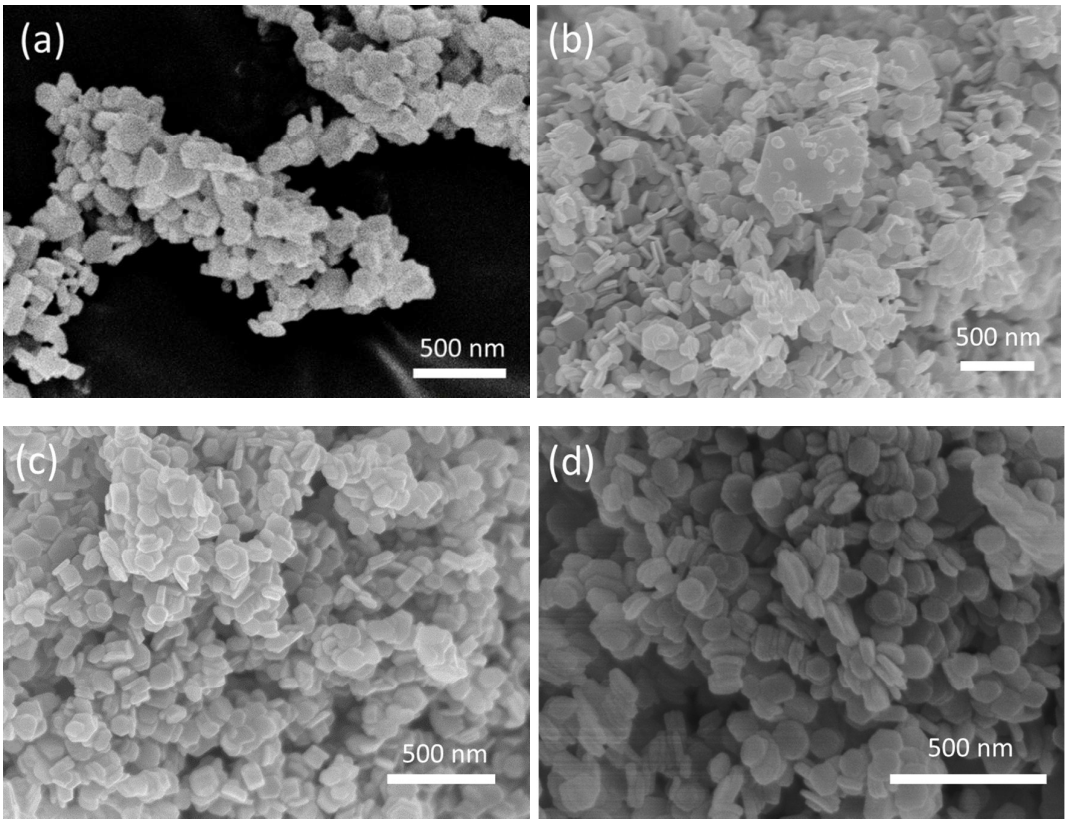

Fig. 8. SEM images of MgO samples synthesised with NaOH and different SDS concentrations; (a) **A0c**, (b) **A1c**, (c) **A2c** and (d) **A4c**.

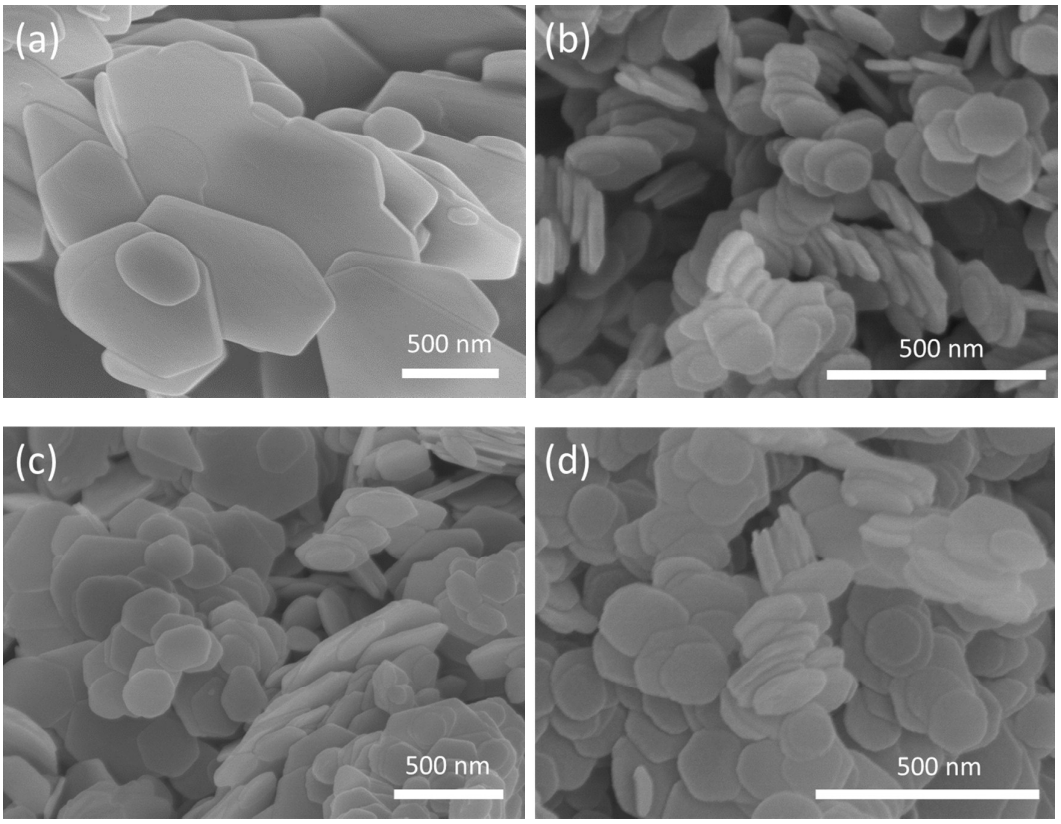

Fig. 9. SEM images of MgO samples synthesised with TPAOH and different SDS concentration; (a) **B0c**, (b) **B1c**, (c) **B2c** and (d) **B4c**.

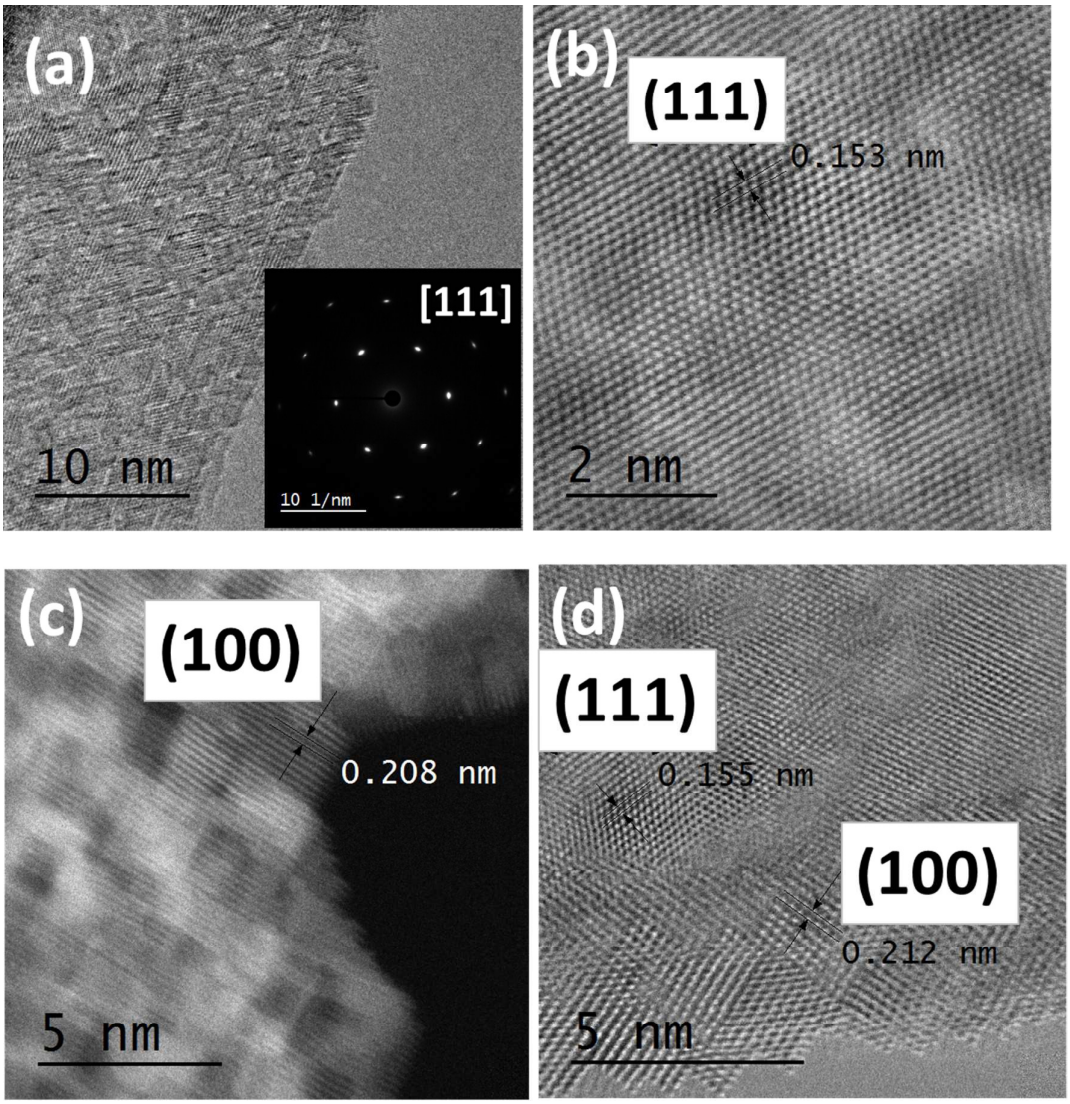

Fig. 10. HRTEM images of MgO samples synthesised with TPAOH and different SDS concentration; **B0c** (a-b) and **B4c** (c-d).

Surfactant controlled magnesium oxide synthesis for base catalysis.

Nicholas F. Dummer[a,b]*, Liam Joyce[a], Harold Ellicot[a], Yijiao Jiang[c]

[a] School of Chemistry, University of Wollongong, Wollongong, NSW 2522, Australia

[b] Now at Cardiff Catalysis Institute, Cardiff University, Cardiff, CF10 3AT, UK

[c] Department of Engineering, Macquarie University, North Ryde, NSW 2109, Australia

* Corresponding author; dummernf@cardiff.ac.uk

Graphical Abstract